

Los Alamos National Laboratory is operated by the University of California for the United States Department of Energy under contract W-7405-ENG-36

TITLE: Ablation of Material by Front Surface Spallation

AUTHOR(S): R. S. Dingus and R. J. Scammon

JUL 0 1991

SUBMITTED TO OFRL Workshop on Laser Ablation--Mechanisms and Applications Conference Proceedings, Oak Ridge, TN, 8-10 April, 1991, to be published by Springer-Verlag

DISCLAIMER

This report was prepared as an account of work sponsored by an agency of the United States Government. Neither the United States Government nor any agency thereof, nor any of their employees, makes any warranty, express or implied, or assumes any legal liability or responsibility for the accuracy, completeness, or usefulness of any information, apparatus, product, or process disclosed, or represents that its use would not infringe privately owned rights. Reference herein to any specific commercial product, process, or service by trade name, trademark, manufacturer, or otherwise does not necessarily constitute or imply its endorsement, recommendation, or favoring by the United States Government or any agency thereof. The views and opinions of authors expressed herein do not necessarily state or reflect those of the United States Government or any agency thereof

By acceptance of this article the publisher recognizes that the U S Government retains a nonexclusive, royalty-free license to publish or reproduce the published form of this contribution or to allow others to do so for U S Government purposes

The Los Alamos National Laboratory requests that the publisher identify this article as work performed under the auspices of the U S Department of Energy

MASTER

Los Alamos

Los Alamos National Laboratory
Los Alamos, New Mexico 87545

COPIES OF THIS DOCUMENT IS UNLIMITED



ABLATION OF MATERIAL BY FRONT SURFACE SPALLATION

R. S. Dingus and R. J. Scammon

Los Alamos National Laboratory, Los Alamos, NM 87545

ABSTRACT

Laser irradiation can be utilized to remove (i.e., ablate) material in a controlled manner by a hydrodynamic process, referred to as front surface spallation. In this process, a thin layer next to a free surface is heated to a level (below vaporization) so rapidly that it cannot undergo thermal expansion during laser heating. This generates a stress pulse, which propagates both inward and toward the free surface, with an initial amplitude that can be calculated using the Grüneisen coefficient. As the pulse reflects from the free surface, a tensile tail can develop of sufficient amplitude, exceeding the material strength, that a layer will be spalled off, taking much of the laser-deposited energy with it. To achieve spallation conditions, the laser wavelength, pulselength and fluence must be tailored to the absorption depth, Grüneisen coefficient, and spall strength. Hydrodynamic calculations and analytical modeling are presented to explain the process and illustrate conditions under which it should be expected to occur. Under some conditions, front surface spallation can have advantages over ablation by thermal vaporization, where residual temperatures are generally higher.

1. INTRODUCTION

The information in this paper has been derived from efforts to develop computational techniques to model x-ray- and laser-target interaction for defense applications. The effort has included the performance of detailed experiments to gain confidence in the modeling. The knowledge gained from these efforts appears to have potential benefit to medical and other industrial applications. The computational modeling efforts have involved development of a basic understanding of the processes along with simple analytical codes; development of large, numerical, radiation-hydrodynamic-computer codes to analyze complex conditions; and development of the necessary materials properties data bases for these calculations. The discussion in this paper will emphasize semi-transparent materials, with a vacuum or gas in front, exposed to short pulselength lasers with fluences just above the ablation threshold. The laser wavelength will be assumed to be long enough that breakage of molecular bonds by photon absorption is not a dominant process. More general discussions of pulsed laser effects phenomenology are presented in Ref. 1-5.

A reasonable criterion for being semi-transparent is that a significant fraction, if not all, of the laser beam is absorbed in the material, but the laser pulselength is short enough that the laser penetration depth is larger than the depth to which energy is transported by thermal diffusion during the time of the laser pulse. For rapid heating, when the front surface dose is above the complete vaporization energy (i.e., ΔH_C , the energy per unit mass to take the material from its

ambient temperature into the vapor state), material will be ablated by vaporization to a depth at which the dose equals the complete vaporization energy. A fraction of the material with a dose above the incipient vaporization energy (i.e., ΔH_i , the energy to take the material to the vaporization temperature, but excluding the latent heat of vaporization, ΔH_v ; $\Delta H_c = \Delta H_i + \Delta H_v$; generally $\Delta H_i \ll \Delta H_v$) will also be vaporized. This vapor can entrain nonvaporized material from this region so that the precise amount of material ablated from this region is dependent on rates including those associated with both thermodynamics and hydrodynamics. As the heating pulse length gets longer (for semi-transparent materials), the situation becomes more complicated because there is time for cooling by ablation to peg the front surface temperature at the vaporization temperature, while in depth laser heating can cause superheating until instabilities result in rapid vaporization at some depth, which will drive off cooler material at lesser depths. For opaque materials, this will not occur because the heating source remains at the surface

2. FRONT SURFACE SPALLATION PROCESS

For semi-transparent materials, if the laser pulse length and the time for conversion of absorbed laser energy to thermal energy are sufficiently short, such that the transit distance of an acoustic signal during the laser pulse is less than or of the order of one laser absorption depth, then the heating from laser absorption will induce a stress pulse whose amplitude is proportional to the absorbed fluence. At fluences below that for thermal vaporization, this stress pulse can cause front surface spallation, which is a form of ablation. This type of ablation generally requires less fluence per unit mass ablated than is required by ablation from thermal vaporization or photochemical decomposition because the material is ejected in solid or liquid fragments rather than as molecules or atoms, which requires more energy to break more bonds. For short laser pulse lengths (i.e., large laser flux), large compressive stress pulses can be imparted to the material by thermal vaporization or photochemical decomposition due to the rapidity with which the momentum of the ablated material is carried away.

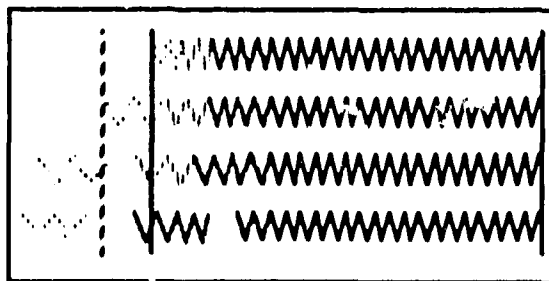


Figure 1. Illustration of front surface spallation process.

Figure 1 illustrates the basic process relating to front surface spallation. Imagine that the material of interest is a spring with a certain compressibility; Fig. 1 shows four configurations of this spring. Suppose that the front surface of the material (spring) is heated to some depth

during a short time as illustrated by the hatched portion of the spring at the top in the figure. If the material had been heated slowly, thermal expansion would have caused it to expand to the vertical dotted line to the left in Fig. 1, as shown in the next spring down. However, because it was heated so rapidly, it acquires a significant velocity during the expansion (provided it is not restrained by another material in contact), which must be followed by deceleration to bring it back to rest. If the material has insufficient strength, the force associated with the deceleration will cause a fracture and a layer will keep going as shown by the next case. This fracture is referred to as spallation, or spall for short. Depending on the circumstances, the velocity of the residual material can cause one or more additional layers to spall as shown for the bottom spring.

Front surface spallation can also be described in more quantitative, but equivalent terms. Heating a (front surface) layer of material before it can thermally expand causes a (positive) compressive stress pulse in that region whose amplitude can be calculated using the Grüneisen coefficient. This stress pulse will cause dynamic expansion, both toward the front surface and in the opposite direction. The stress pulse will be reflected at the front surface by the shock impedance mismatch producing a reflected (negative) tensile pulse, if the impedance of the material in front is less than that of the material. To have spall, it is generally necessary that the material in front of the material be a gas or vacuum and not a liquid or solid; otherwise, the shock impedance of the material in front will prevent a tensile wave of sufficient amplitude from developing. The tensile pulse trails the compressive pulse into the material, thus causing the characteristic bipolar stress pulse seen in stress measurements at low fluences⁶. If at some depth, the tensile stress exceeds the tensile spall strength of the material, then the material will spall at that depth, creating a new boundary surface at which the stress becomes zero. The rest of the compressive pulse that is propagating toward the front surface will then be reflected from this new boundary. If the reflected tensile stress builds up to the spall stress again, then spall will occur again. Eventually, the criterion will no longer be met for another spall layer to develop and a residual tensile tail will be left in the material with an amplitude that is less than the spall strength of the material.

3. EQUATIONS FOR THERMOELASTIC STRESS

To understand the basic relations governing the spallation process, a purely thermoelastic response of the material is assumed along with an exponential laser deposition profile and constant absorption coefficient, μ . For the sake of discussion, it is assumed that the deposited laser energy is instantly converted into heat. The time scale is assumed to be short enough that thermal conduction can be ignored; however, it is assumed that the heat is distributed locally uniformly where it is deposited. The laser beam is assumed to expose a large diameter of material compared to the absorption depth.

For an incident fluence, F_0 , into the material (after correction for reflection at the material surface), the fluence, F , at a depth x in the material is given by $F = F_0 \exp(-\mu x)$. The energy density (energy per unit mass), E , deposited by the laser in the material at depth x is $E = -(1/\rho) dF/dx = (\mu/\rho) F_0 \exp(-\mu x)$. A rectangular step function laser temporal profile is assumed with a pulselength, τ_L , because it is most illustrative. Other pulse shapes can also be treated analytically⁶ and calculations for arbitrary pulse shapes can be done numerically with hydrodynamic codes.

The material properties important to the photospall process are: the absorption coefficient, μ ; the sound speed, c ; the Grüneisen coefficient, Γ ; and the spall strength, σ_s . It is convenient to define a characteristic time, t_0 , where $t_0 = 1/\mu c$, which is the time for an acoustic signal to propagate a distance of one laser absorption depth ($1/\mu$). Also, let τ_L be the ratio of the laser pulselength to this characteristic time, so $\tau_L = \tau_L / t_0 = \mu c \tau_L$. It is instructive to discuss how the stress waveform develops in the material. For simplicity, the sound speed is assumed to be constant (actually at higher compressive stress, the speed is generally slightly higher, but this change is probably negligible for the low stresses and short distances of interest in the present discussion). If the laser energy was deposited instantaneously in the material, the stress, σ , in the material just after deposition would be compressive with an amplitude at a distance x into the material of

$$\sigma = \Gamma \mu F_0 \exp(-\mu x) \quad (1)$$

Actually, because the front surface is a free surface (it is assumed that a gas, which has a shock impedance of essentially zero, or a vacuum is outside the front surface), the stress must be zero for all time at $x = 0$; this boundary condition is insured by the ensuing reflection at this surface. The stress pulse immediately begins to propagate both toward the surface and away from the surface with a velocity c . This bifurcation in direction, leads to a factor of two reduction in amplitude. For illustrative purposes, one can think of the stress given in Eq. 1 as consisting of two pulses, each with half the amplitude of Eq. 1; one moving inward, the other outward. At any given time, the stress is the superposition of these two pulses. The inward moving pulse simply translates with velocity c . Each element of the outward moving pulse reverses sign and direction as it reflects from the front surface. This results in a bipolar stress pulse, which, at any given time t , makes an abrupt transition at the location ct in the material from the largest tensile value to the largest compressive value. For times of the order of or less than the characteristic time, t_0 , the peak tensile stress is building asymptotically from zero to its maximum negative value of $-\Gamma\mu F_0/2$, while the peak compressive stress is decreasing asymptotically from $+\Gamma\mu F_0$ to $+\Gamma\mu F_0/2$. During times for which $t \gg t_0$, the stress amplitude decreases from the peak stress value, σ_p , to zero exponentially as $\exp(-\mu|x'|)$ in both directions, where $|x'|$ is the distance from the location ct . Because of the assumed linear elastic

the stress as a function of time at given positions in the material. It is interesting to note that nowhere in this paper are the processes under discussion dependent on a shock front⁵ developing in the material.

If the laser has a finite pulselength, τ_L , then stress propagation occurs during the pulse causing a number of differences from instantaneous energy deposition. For a rectangular step function laser temporal profile (as is being assumed), the tensile stress does not begin to develop until the laser pulse ends. During times for which $t \gg t_0$, and $t \gg \tau_L$, the tensile and compressive stress peaks become separated by a distance $c\tau_L$ and the peak stress value, σ_p , is reduced by a factor A , which accounts for the stress relief that occurs during the laser pulse, where $A = (1 - \exp(-\tau_L)) / \tau_L$. This attenuation factor approaches 1 as τ_L goes to zero and approaches $1 / \tau_L$ for large values of τ_L . The factor A is plotted versus τ_L in Fig. 2. As illustrated in Fig. 2, the peak stress is reduced substantially when τ_L is greater than one.

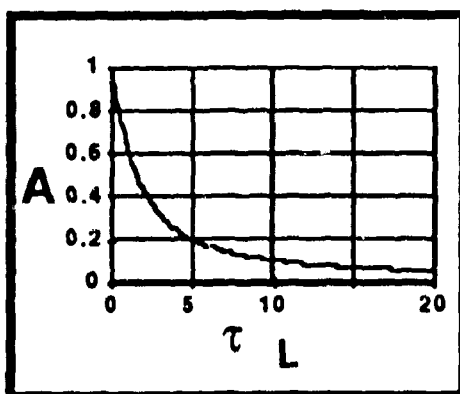


Figure 2. Stress attenuation versus ratio of laser pulselength to characteristic time.

Thus, the peak tensile stress, σ_p , developed in the material occurs (assuming no spall) at times late compared to the laser pulse duration, τ_L , and late compared to the characteristic time, t_0 , and has an amplitude of

$$\sigma_p = (A/2) \Gamma \mu F_0 \quad \text{for } t \gg \tau_L \text{ and } t \gg t_0. \quad (2)$$

It is interesting to note that, when $\tau_L \gg 1$, then σ_p is inversely proportional to τ_L and independent of μ ; that is,

$$\sigma_p \approx (1/2) \Gamma F_0 / (c\tau_L) \quad \text{for } t \gg \tau_L, \quad t \gg t_0 \text{ and } \tau_L \gg 1. \quad (3)$$

To better understand the origin of the stress, it is helpful to examine the terms in Eq. 2. The Grüneisen coefficient can be written as $\Gamma = \beta / (\rho C_v \kappa_T)$ where β is the thermal expansion coefficient, ρ is the density, C_v is the specific heat at constant volume and κ_T is the isothermal compressibility of the material. Putting this into Eq. 2 gives $\sigma_p = (A/2)(1/\kappa_T)\beta(\mu/\rho)F_0 / C_v$. The product $(\mu/\rho)F_0$ gives the peak laser dose in energy per unit mass, which occurs at the

front surface of the material; dividing this by C_V gives the temperature rise; multiplying this by β gives the thermal expansion; multiplying this by $1/\kappa_T$ gives the stress caused by this thermal expansion; multiplying this by $1/2$ accounts for the stress propagating both inward and outward as discussed above; and multiplying this by A corrects for stress propagation during the laser pulse.

Equation 2 assumes a Mie-Grüneisen equation of state, which is applicable for the solid and liquid phases. At high fluences where vaporization occurs (i.e., $(\mu/\rho)F_0 > \Delta H_i$), as the vapor expands, the equation of state more nearly approximates that of an ideal gas.

In reality it takes a finite time for materials to fracture when subjected to a tensile stress; fracture models have been developed to account for this complication⁷. Neglecting this complication for now, if the spall strength of the material is less than the peak tensile stress, then the material will spall at the location and time in the material where and when the peak stress reaches the spall strength. Thus, spall occurs if $\sigma_p > \sigma_s$. After the spallation occurs, depending on the circumstances, the tensile stress may build again to the spall strength amplitude, spalling off another layer. The total number of spall layers is approximately one to two times the ratio σ_p / σ_s and the total spall depth is approximately one to a few times the laser absorption depth ($1/\mu$). These relations for the number of spall layers and the spall depth are not exact principally because part of the tensile stress pulse generally will have propagated beyond the spall location by the time of each spall and because of the discrete nature of the spallation process in association with an exponentially increasing stress with distance into the material.

4. ANALYTIC THERMOELASTIC STRESSWAVE CALCULATIONS

Let $\tau = \mu ct$, $\tau_L = \mu ct_L$, and $\xi = \mu x$. Then, assuming that the laser flux is constant for a duration of t_L and with a total fluence of F_0 , evaluating the integrals presented in the paper by Bushnell⁸ gives.

$$\sigma = (1/(2\tau_L)) \Gamma \mu F_0 [\exp(-(\tau - \xi)) - \exp(-(\tau + \xi))] \quad \text{for } \tau \leq \tau_L, \xi \leq \tau \quad (4)$$

$$\sigma = (1/(2\tau_L)) \Gamma \mu F_0 [\exp(-(\xi - \tau)) - \exp(-(\xi + \tau))] \quad \text{for } \tau \leq \tau_L, \xi \geq \tau \quad (5)$$

$$\sigma = -(A/2) \Gamma \mu F_0 [\exp(-(\tau - \tau_L - \xi)) - \exp(-(\tau - \tau_L + \xi))] \quad \text{for } \tau \geq \tau_L, \xi \leq \tau - \tau_L \quad (6)$$

$$\sigma = -(A/2) \Gamma \mu F_0 [B \exp(-(\tau - \tau_L - \xi)) - \exp(-(\tau - \tau_L + \xi))] \quad \text{for } \tau \geq \tau_L, \tau - \tau_L \leq \xi \leq \tau \quad (7)$$

$$\sigma = (A/2) \Gamma \mu F_0 [\exp(-(\xi - \tau)) + \exp(-(\xi + \tau - \tau_L))] \quad \text{for } \tau \geq \tau_L, \xi \geq \tau \quad (8)$$

$$\text{where } A = (1 - \exp(-\tau_L)) / \tau_L \quad \text{and} \quad B = (\exp(2(\tau - \tau_L - \xi)) - \exp(-\tau_L)) / (1 - \exp(-\tau_L)) \quad (9)$$

Figures 3 and 4 present the results of calculations using Eqs. 4-9, which assume that the

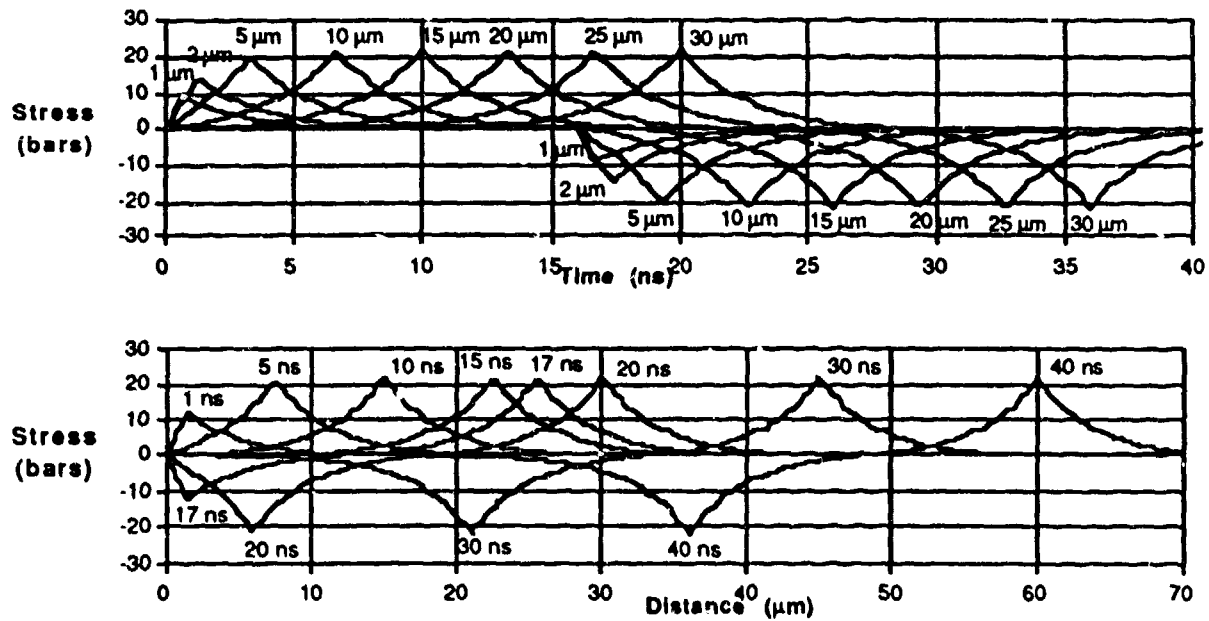


Figure 3. Thermoelastic stresswave development for long laser pulse length compared to characteristic time. Parameters used were: $\mu = 2700 \text{ cm}^{-1}$, $c = 1.5 \text{ } \mu\text{m/ns}$, $\Gamma = 0.15$, $F_0 = 0.07 \text{ J/cm}^2$, $t_L = 16 \text{ ns}$. Resultant values are: $\tau_L = 6.5$, $\sigma_p = 22 \text{ bar}$ and front surface temperature rise is $45 \text{ }^\circ\text{C}$.

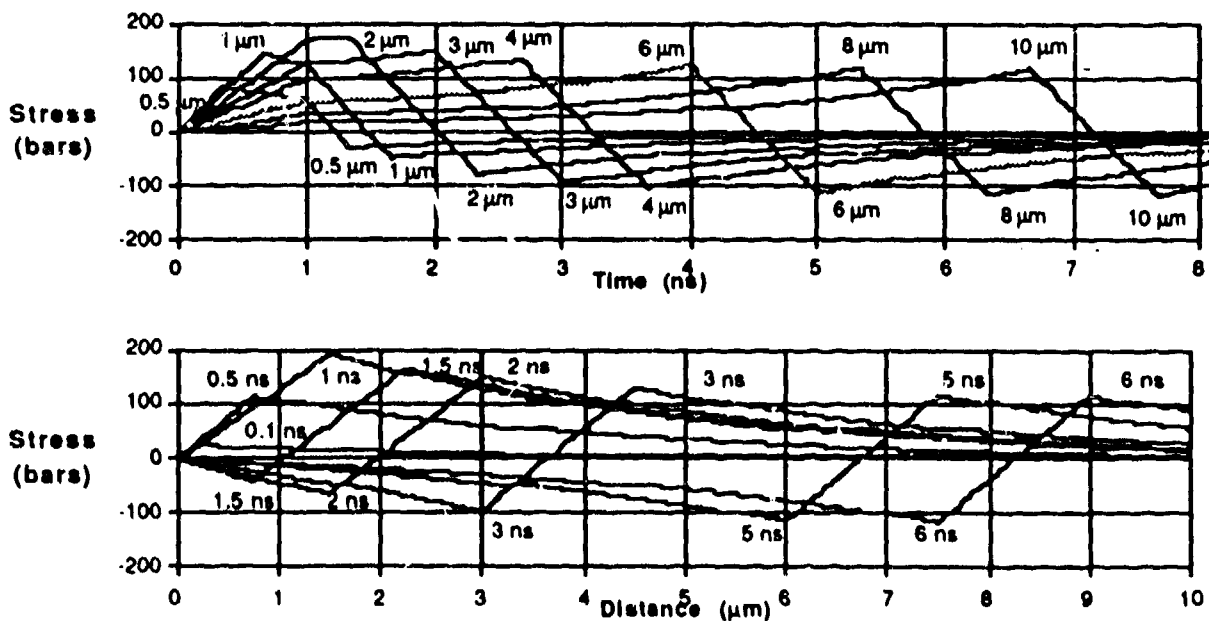


Figure 4. Thermoelastic stresswave development for short laser pulse length compared to characteristic time. Parameters used were: $\mu = 2700 \text{ cm}^{-1}$, $c = 1.5 \text{ } \mu\text{m/ns}$, $\Gamma = 0.15$, $F_0 = 0.07 \text{ J/cm}^2$, $t_L = 1 \text{ ns}$. Resultant values are: $\tau_L = 0.41$, $\sigma_p = 117 \text{ bar}$ and front surface temperature rise is $45 \text{ }^\circ\text{C}$.

spall strength is large enough that spall does not occur. In Fig. 3, the material properties used are those estimated for corneal tissue exposed to a typical ArF laser pulse⁶. Figure 4 is for the same conditions except that the laser pulse length is 1 ns instead of 16 ns. In the top part of Figs. 3 and 4, the stress in the material is plotted as a function of time at different positions in the material. The bottom part of Figs. 3 and 4 gives the stress as a function of position in the material at different times. In these figures, it may be noted that the separation between the positive and negative peaks is equal to the pulse length, that no negative stress develops during the laser pulse and that the peak stress amplitude is much larger for the 1 ns pulse than for the 16 ns pulse as indicated by Eq. 2.

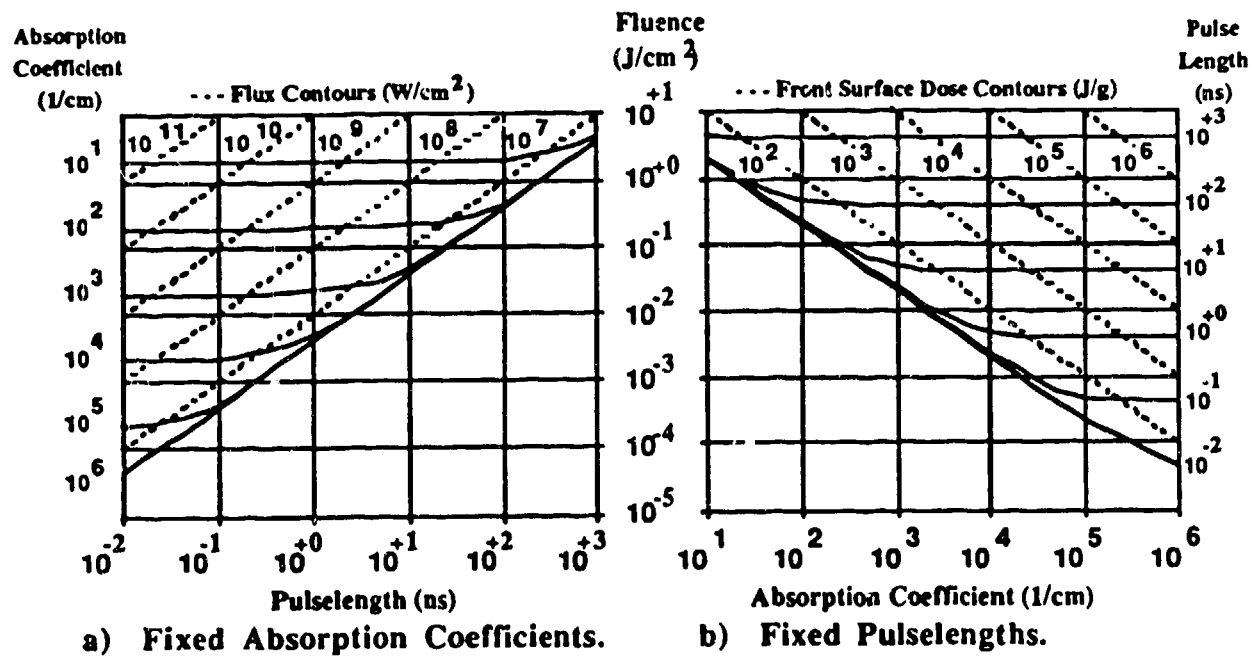


Figure 5. Fluence threshold for front surface spallation calculated from Eq. 2 using $\sigma_s / \Gamma = 100$ bar, $c = 2 \mu m/ns$, and $\rho = 1 g/cm^2$.

Figure 5 gives threshold fluence curves for front surface spallation from Eq. 2 for the specific parameter values indicated (typical of a liquid), plotted as a function of pulselength for various absorption coefficients in Fig. 5 a) and as a function of the absorption coefficient for various pulselengths in Fig. 5 b). The curves can be easily scaled to different parameter values using Eq. 2. For most liquids or solids, the Grüneisen coefficient has a value of the order of 0.3 to 3, the spall strength of solids is of the order of 5 to 50 kbar, and the spall strength of liquids is of the order of 10 to 100 bars⁹. Because the spall strength for liquids is small, front surface spallation will frequently tend to cause ablation of exposed solid targets down to the melt depth. The dashed lines in the Figs. 5 a) and b) are respectively contour lines for constant flux (F_0/t_L) and constant front surface energy deposition ($\mu F_0/\rho$). The threshold fluence

curves in Fig. 5 merge in the vicinity of $\mu\tau_L = 1$ such that for much larger τ_L or μ , the fluence is determined by Eq. 3 (which is independent of μ) and for much smaller τ_L or μ , the fluence is determined by Eq. 2 with $A = 1$ (which is independent of τ_L). For example, Fig. 5 shows that (for the parameters used in Fig. 5) for a fixed absorption coefficient of 10^4 cm^{-1} , the threshold fluence decreases as the pulselength is decreased to about 1 ns, but does not decrease much for shorter pulselengths. Similarly, for a fixed pulselength of 1 ns, the threshold fluence decreases as the absorption coefficient is increased to about 10^4 cm^{-1} , but does not decrease much for larger absorption coefficients. Figure 5 a) and b) respectively show that, for the parameters used, a flux of at least, $4 \times 10^6 \text{ W/cm}^2$ and a front surface dose of at least 20 J/g are required for front surface spall. This flux is not far from that at which aerosol breakdown in air¹ may become a problem so that some experiments of interest might need to be performed in vacuum.

For medical applications where tissue apparently has a reasonably high Grüneisen coefficient and a reasonably small spall strength, front surface spallation should be a possible means of ablation⁵. For aluminum, as an example of a metallic solid, the Grüneisen coefficient is about 1, the melt energy is about 1000 J/g (desirable to drive to melt to reduce spall strength), the penetration depth ($1/\mu$) for optical photons is about 10^{-6} cm , the sound speed is about 5 $\mu\text{m/ns}$, which suggests a pulselength of about 2 ps or less (to keep $\mu\tau_L < 1$). The thermal diffusivity, k , is about $1 \text{ cm}^2/\text{s}$ so that in 2 ps, the thermal diffusion depth ($\delta = \sqrt{4kt}$) is about $3 \times 10^{-6} \text{ cm}$, which exceeds the laser penetration depth, so that Eq. 2 would have to be corrected for thermal diffusion. Although much higher doses would be required than needed in Fig. 5, it appears feasible to ablate very thin layers of metals with very short pulselength optical lasers.

5. HYDRODYNAMIC CODE CALCULATIONS

Figures 6 and 7 present the results of hydrodynamic calculations, using the Chart D code¹⁰ with the laser and material properties shown in those figures, to illustrate how the stress behavior changes when front surface spall occurs. The equation of state used was approximately that for aluminum, but it was artificially changed for illustrative purposes. In Fig. 6, a large spall strength was used so that spall would not occur; the stress is plotted in dynes/cm² ($10^6 \text{ dynes/cm}^2 = 1 \text{ bar}$) as a function of position in the material at times of 1.59 ns, 1.90 ns, 10 ns and 20 ns. In these plots the front surface was at $x = 0.2 \text{ cm}$ and x decreases as the distance into the material increases. In Fig. 7, where a spall strength of 3 kbar was used, the stress is plotted at essentially these same times plus at two additional times. The dashed vertical lines in Fig. 7 indicate the location at which spall planes develop. Spall first occurs at a time of 1.54 ns when the tensile stress reaches 3 kbar. The plot at 1.90 ns shows that the tensile stress has again built up to nearly 3 kbar. The plot at 1.92 ns shows that a second spall plane has developed. At 10 ns, six spall planes have developed and another is about to occur. At 10.9 ns, the seventh and last spall plane has occurred. After spall, the residual stress pulse in each spall layer reflects repeatedly within that layer. The momentum of each spall layer is about

APPROXIMATE ALUMINUM EOS
artificial parameters

$\mu = 300 \text{ cm}^1$ $\Gamma = 2.5$ $t_L = 0.65 \text{ ns}$ for illustrative purposes
 $c = 5.17 \text{ } \mu\text{m/ns}$ $F_0 = 3.6 \text{ J/cm}^2$ $\tau_L = 0.1$ Spall Strength = ∞

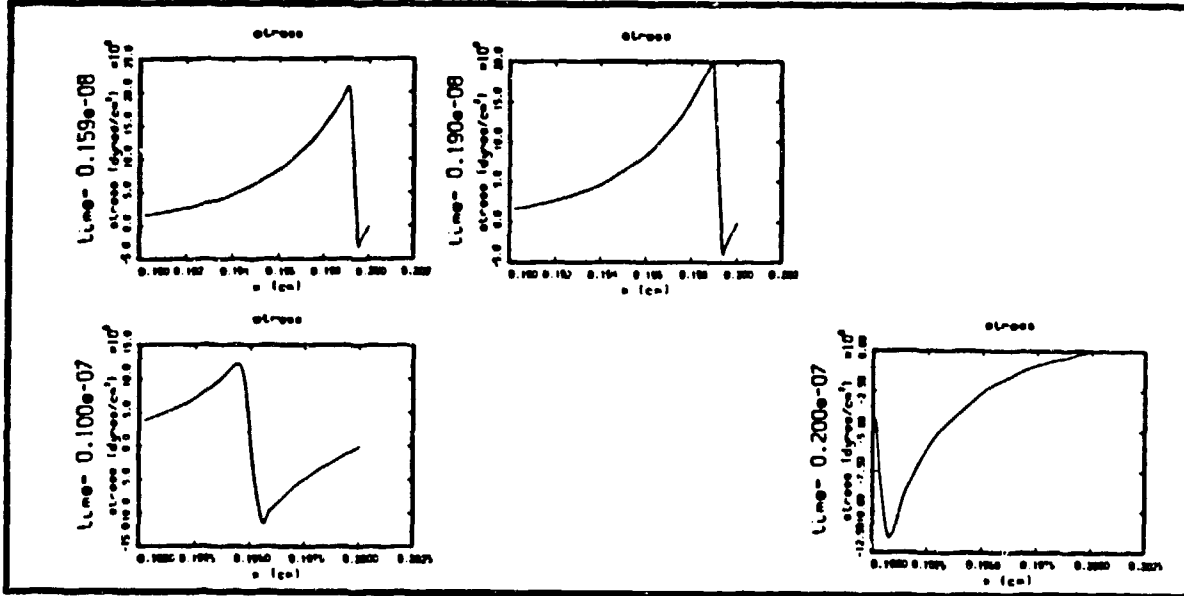


Figure 6. Hydrodynamic code calculations for no front surface spallation.

APPROXIMATE ALUMINUM EOS
artificial parameters

$\mu = 300 \text{ cm}^1$ $\Gamma = 2.5$ $t_L = 0.65 \text{ ns}$ for illustrative purposes
 $c = 5.17 \text{ } \mu\text{m/ns}$ $F_0 = 3.6 \text{ J/cm}^2$ $\tau_L = 0.1$ Spall Strength = 3 kbar

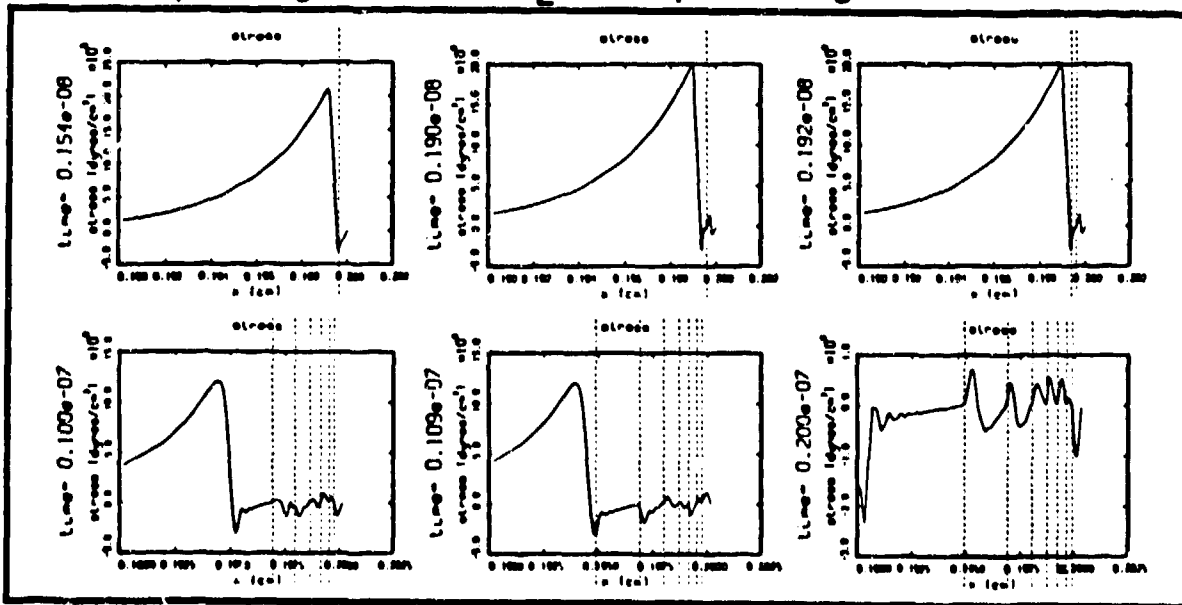


Figure 7. Hydrodynamic code calculations with front surface spallation.

the same, but the thickness increases exponentially with successive layers so that the velocity decreases exponentially with successive layers. This signature might be something to look for experimentally. The position, x , in Figs. 6 & 7 is a Lagrangian coordinate (which is fixed to the mass elements rather than representing location in space) so that the gaps between spall layers do not appear in the plots.

6. SUMMARY

Front surface spallation is a potential mechanism for laser ablation of materials that may have a number of significant applications, such as medical surgery⁵. Perhaps it could be used also for desorption or to launch material (for example, large biological molecules) from a surface into a region where other techniques might be used to study the launched material or, for example, to vaporize it for production of superconducting thin films. It might also have value in cutting or shaping materials including precision etching such as for lithography.

7. REFERENCES

1. A. N. Pirri, *Theory for momentum transfer to a surface with a high-power laser*, Physics of Fluids, Vol. 16, no. 9, pp. 1435-1440, 1973.
2. R. S. Dingus and S. R. Goldman, *Plasma energy balance model for optical-laser induced impulse in vacuo*, Proceedings of the International Conference on Lasers '86, pp. 111-122, Orlando, Florida, 1986.
3. R. S. Dingus et al, *Pulsed Laser Effects Phenomenology*, in M. J. Berry and G. M. Harpole, editors, SPIE Proceedings of Thermal and Optical Interactions with Biological and Related Composite Materials, Vol. 1064, 1989.
4. R. S. Dingus and B. P. Shafer, *Laser-induced shock wave effects in materials*, SPIE Proceedings of Laser-Tissue Interaction, Vol. 1202, 1990.
5. R. S. Dingus and R. J. Scammon, *Grüneisen-stress induced ablation of biological tissue*, to be published in SPIE Proceedings of Laser-Tissue Interaction II, Vol. 1427, 1991.
6. P. E. Dyer and R. K. Al-Dhahir, *Transient photoacoustic studies of laser tissue ablation*, Proceedings of Laser-Tissue Interaction, SPIE Vol. 1202, 1990.
7. F. R. Tuler and B. M. Butcher, *A criterion for the time dependence of dynamic fracture*, J. of Fracture Mech. 4-4, 431-437, Dec, 1968.
8. J. C. Bushnell and D. J. McCloskey, *Thermoelastic stress production in solids*, J. Appl. Phys. 39, 5541-5546, 1968.
9. S. L. Thompson and H. S. Lauson, *Improvements in the CHART D Radiation-Hydrodynamic Code II: A Revised Program*, SC-DR-710715, Sandia Laboratories, Albuquerque, NM, February 1972.
10. D. E. Grady, *The Spall Strength of Condensed Matter*, J. Mech. Phys. Solids 36:3, 353-384 (1988)